

## Zn<sub>2</sub>Al Layered Double Hydroxides Intercalated with Nitrate and *p*-Aminobenzoate as Ultraviolet Protective Agents in Low-Density Polyethylene Nanocomposites and Natural Insulating Oils

Neffe A. G. Gómez,<sup>a</sup> Gabriel M. Silva,<sup>a</sup> Helena M. Wilhelm<sup>b</sup> and Fernando Wypych<sup>b</sup> \*<sup>a</sup>

<sup>a</sup>Centro de Pesquisas em Química Aplicada (CEPESQ), Departamento de Química, Universidade Federal do Paraná (UFPR), CP 19032, 81531-980 Curitiba-PR, Brazil

<sup>b</sup>Vegoor Tecnologia Aplicada, 83403-150 Colombo-PR, Brazil

Zn<sub>2</sub>Al-Cl and Zn<sub>2</sub>Al-NO<sub>3</sub> layered double hydroxides (LDHs) were synthesized through the fixed pH co-precipitation method and used as precursor materials for the intercalation of *p*-aminobenzoate through anion exchange reactions. Since chloride in Zn<sub>2</sub>Al-Cl was only partially exchanged with *p*-aminobenzoate, the phases Zn<sub>2</sub>Al-NO<sub>3</sub> and Zn<sub>2</sub>Al-N-AB (nitrate exchanged with *p*-aminobenzoate) were used in different percentages as functional fillers to produce nanocomposites of low-density polyethylene doped with maleic anhydride (LDPE). Analysis of thermal properties showed that the melting and recrystallization temperatures were slightly increased in the nanocomposite containing 5 wt.% Zn<sub>2</sub>Al-N-AB. Weathering tests performed with neat LDPE and the nanocomposite films showed that the addition of the LDHs improved ultraviolet (UV) absorption and reduced the LDPE degradation by 25 and 76% when using Zn<sub>2</sub>Al-NO<sub>3</sub> and Zn<sub>2</sub>Al-N-AB, respectively, as fillers, showing a promising UV-shielding effect. Preliminary results also showed a potential application of Zn<sub>2</sub>Al-N-AB as antioxidant in natural insulating oils (natural ester FR3 and castor oil), opening new opportunity of applications.

**Keywords:** layered double hydroxide, *p*-aminobenzoate, exchange reactions, ultraviolet absorption, polyethylene, nanocomposite

### Introduction

Low-density polyethylene (LDPE) is a crystalline polymer (50-60% of crystallinity) that can be processed by extrusion and injection molding. In normal conditions, LDPE is nontoxic and may be used in contact with food and pharmaceutical products, in films for industrial and agricultural packaging, toys and household appliances, wire and cable insulation, tubes and hoses. LDPE is slowly attacked by oxidizing agents, as normally happens to other polymers that suffer degradation. This degradation is usually induced by factors such as the ultraviolet (UV) radiation in sunlight, high temperatures, presence of photodegradative enhancers, additives and even by the effects of its own molecular weight, which is problematic due to the usage of this polymer, e.g., in electric cables frequently exposed to weathering factors.<sup>1-6</sup> To avoid such problems, anti-oxidants and stabilizers are normally used to improve the resistance, but impurities generated during the polymer processing can also increase its degradation.<sup>1</sup>

Layered double hydroxides (LDHs) are a typical class of layered materials, frequently called hydrotalcite-like materials. The structure of LDHs is similar to brucite [Mg(OH)<sub>2</sub>], consisting of a close hexagonal packing of hydroxide ions of octahedral sites occupied by Mg<sup>2+</sup> ions, sharing edges to build two-dimensional layers that are packed along the basal axis.<sup>7-9</sup> When part of the M<sup>2+</sup> metals in the layers are replaced by M<sup>3+</sup> metals with appropriate ionic radius, the positively charged layers need to be charge-balanced by the intercalation of anions between the layers. The general formula to express these compounds is [M<sub>1-x</sub><sup>2+</sup>M<sub>x</sub><sup>3+</sup>(OH)<sub>2</sub>](A<sup>n-</sup>)<sub>x/n</sub>·mH<sub>2</sub>O, where the cations M<sup>2+</sup> and M<sup>3+</sup> are divalent and trivalent metal ions, respectively, A<sup>n-</sup> is the interlayer anion compensating the excess positive charge, x is an adjustable value (0.2-0.4) and m is the number of water molecules hydrating the anions.<sup>10,11</sup> LDHs have been extensively studied for various possible applications. They have several advantages, such as non-toxicity, adjustable particle size in order to produce homogeneous mixtures with other materials, and simple and cheap synthesis methods. Recently, they have been

\*e-mail: wypych@ufpr.br

used to prepare multifunctional polymer-matrix composites with mixed organic and inorganic properties.<sup>11-14</sup> Several UV absorbers have been intercalated between LDH layers, improving the thermal stability of the guest chromophores and exhibiting enhanced UV photostability.<sup>2,15</sup>

Different papers<sup>2,10,14,16</sup> have been published about Zn<sub>2</sub>Al LDH, reporting that this compound improved the UV radiation absorption property after intercalation of *p*-aminobenzoate (*p*-AB anion). The *p*-AB anion (Figure 1a) is an organic species that interacts with the electromagnetic radiation in the UV region through electronic transitions throughout the molecular orbitals of its chromophoric groups, such as the benzene ring and the carboxylate group, which contribute to the  $\pi$ -conjugated system in the anion (Figure 1b).

As observed in a previous work by our research group,<sup>16</sup> the use of an organic anion intercalated in a cobalt layered compound as filler in LDPE increased the degradation of the polymer due to weathering. For that reason, in this study we analyzed whether after intercalation of *p*-AB in LDH, and using this compound as filler in LDPE to produce a polymer nanocomposite, the UV absorption property would be improved, by evaluating its behavior in response to radiation and verifying if the composite's mechanical properties and thermal stability could also be influenced.

Just as the degradation of polymeric materials is favored by the process of free radical formation in the presence of air, the most common cause of chemical aging of insulating oils is oxidation, so inhibitors need to be used, such as 2,6-di-*tert*-butylphenol or 2,6-di-*tert*-butyl-*p*-cresol to slow the rate of oxidation.<sup>17</sup> In order to determine the influence of the organic UV absorbent into the LDH nanocomposites on commercial natural insulating oils, evaluating their oxidation catalytic activity when compared with UV unsupported absorbers, we decided also to extend the study by performing preliminary conductivity measurements of natural ester insulating fluid containing Zn<sub>2</sub>Al-N-AB.

## Experimental

The chemicals were of analytical grade purity and used without further purification. Vetec (Rio de Janeiro, Brazil) supplied AlCl<sub>3</sub>·6H<sub>2</sub>O and Al(NO<sub>3</sub>)<sub>3</sub>·9H<sub>2</sub>O as well as NaOH. Biotec (Pinhais, Brazil) supplied ZnCl<sub>2</sub> and Zn(NO<sub>3</sub>)<sub>2</sub>·6H<sub>2</sub>O while Sigma-Aldrich (Saint Louis, USA) supplied *p*-aminobenzoic acid (PABA). LDPE 600 BA (melt flow index (MFI) 21 g 10 min<sup>-1</sup> and density 0.924 g cm<sup>-3</sup>), a resin free of additives, was obtained from ExxonMobil (Texas, USA). SCONA SCONA TPPE 1003 GALL (Wesel, Germany) is based in maleic anhydride monomer grafted to polyethylene (MSA) and was used as compatibilizing agent to try to improve the interaction between additives and the polymeric matrix.

For the synthesis of Zn<sub>2</sub>Al-NO<sub>3</sub> through co-precipitation at fixed pH, Al(NO<sub>3</sub>)<sub>3</sub>·9H<sub>2</sub>O (50 mmol) and Zn(NO<sub>3</sub>)<sub>2</sub>·6H<sub>2</sub>O (100 mmol) were mixed and dissolved in 200 mL of deionized and decarbonated water. The metal salt solution was simultaneously dripped with a NaOH solution (1.0 mol L<sup>-1</sup>) in a beaker for 3 h under constant magnetic stirring, keeping the pH close to 8.0. The slurry was kept under stirring for 24 h at room temperature. Then the precipitate was centrifuged and the solid was repeatedly washed with deionized water and dried in a vacuum oven for 4 days at 60 °C (Zn<sub>2</sub>Al-NO<sub>3</sub>). The same method was followed to prepare the precursor Zn<sub>2</sub>Al-Cl from ZnCl<sub>2</sub> (100 mmol) and AlCl<sub>3</sub>·6H<sub>2</sub>O salts (50 mmol). Both reactions were performed under N<sub>2</sub> flow to avoid contamination with carbonate from atmospheric CO<sub>2</sub>.

For the exchange reactions with *p*-aminobenzoate (*p*-AB), 100 mmol of PABA were previously neutralized with 100 mL of a 1 mol L<sup>-1</sup> NaOH solution. 3.0 g of the precursor Zn<sub>2</sub>Al-NO<sub>3</sub> were added in the *p*-aminobenzoate solution (2.5 mol L<sup>-1</sup>) under magnetic stirring for 5 days, followed by vacuum filtration and washing with deionized water/ethanol (1:1) solution. The yellowish material was dried in a vacuum oven for 5 days at 50 °C (Zn<sub>2</sub>Al-N-AB).

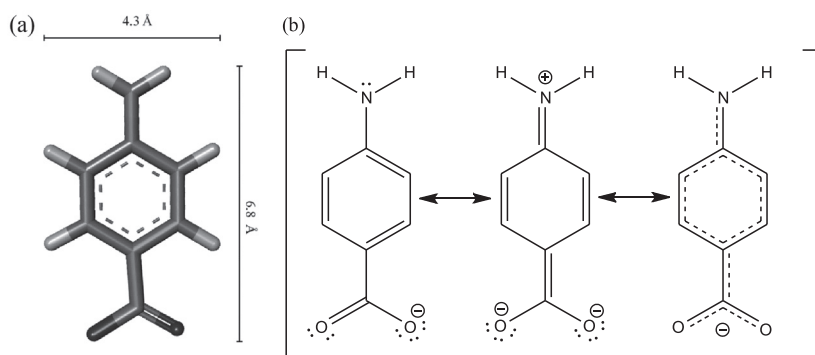


**Figure 1.** Schematic structure and dimensions of the *p*-aminobenzoate anion: (a) stick molecular model optimized with B3LYP/6-31G theory level and (b) some of the canonical structures of the  $\pi$ -resonance system according to the Lewis structure.

From the precursor  $Zn_2Al-Cl$ , the exchange reaction was performed after mixing 3.0 g of the precursor with the *p*-aminobenzoate solution ( $2.5 \text{ mol L}^{-1}$ ) under stirring at  $50 \text{ }^\circ\text{C}$ . The dispersion was kept under stirring for 5 days, followed by centrifugation and washing with deionized water. The solid was dried at  $60 \text{ }^\circ\text{C}$  for 3 days, resulting in a slightly yellowish material ( $Zn_2Al-Cl-AB$ ).

For the nanocomposites, first a masterbatch was obtained using  $Zn_2Al-NO_3$  or  $Zn_2Al-N-AB$ . The layered materials were added to LDPE/MSA and the mixture was fed into a HAAKE MiniLab II micro compounder. The specimens were prepared by melting the LDPE/LDH mixture at  $190 \text{ }^\circ\text{C}$  and 100 rpm, using a co-rotating twin-screw extruder ( $15 \text{ cm}^3$  micro compounder, DSM Xplore). The polymer cord was then removed from the extrusion machine at  $184 \text{ }^\circ\text{C}$ . Next, the masterbatch was diluted in LDPE to obtain samples with different LDH ratios (1, 2, 3, 4, 5 wt.%). Since only small sample amounts could be used in the weathering test, only the nanocomposite containing 5 wt.% filler was used to prepare  $50 \text{ }\mu\text{m}$  thick polymer films after pressing the material in a fusing press at  $190 \text{ }^\circ\text{C}$ . The use of 5 wt.% to prepare composites is reported to be appropriate to maintain the UV-stability of antioxidant anions (intercalated in LDH) in different polymers.<sup>18,19</sup>

X-ray powder diffraction (XRD) patterns were recorded using a Shimadzu XRD6000 diffractometer with  $Cu \text{ K}\alpha$  ( $\lambda = 1.5418 \text{ \AA}$ ) radiation, dwell time of  $2^\circ \text{ min}^{-1}$ , 30 mA and 40 kV. The samples were placed on aluminum sample holders. The polymer films were analyzed allocating the material in an aluminum sample holder with a cavity in the middle, and to correct any reflection displacements, a small amount of silicon powder was used as an internal standard.

Fourier-transform infrared spectroscopy (FTIR) spectra were acquired with Bio-Rad FTS 3500GX and Bomem Michelson MB 100 spectrophotometers, operating in transmission mode with 32 scans with a nominal resolution of  $2 \text{ cm}^{-1}$ . The powder samples were mixed with spectroscopic grade KBr in pellets pressed at 10 tons, and polymer composites were used as films using the same sample holder. Due to the fragility of the nanocomposites films after the weathering tests, the FTIR measurements were only possible by transmission mode.

Thermal analyses (thermogravimetry (TGA) and differential scanning calorimetry (DSC)) of powder samples were carried out using 0.065 mL alumina crucibles with a Netzsch STA 449 F3 series EP analyzer, under synthetic air flow of  $50 \text{ mL min}^{-1}$  and heating rate of  $10 \text{ }^\circ\text{C min}^{-1}$ , in the range of 30 and  $1000 \text{ }^\circ\text{C}$ .

Thermogravimetric analyses (TGA) of nanocomposite samples were performed with a heating rate of  $10 \text{ }^\circ\text{C min}^{-1}$  using a TGA Q5000 analyzer from TA Instruments in an

inert nitrogen atmosphere in the temperature range of  $25\text{-}700 \text{ }^\circ\text{C}$ .

The measurements by scanning electron microscopy (SEM) combined with energy dispersive spectroscopy (EDS) were conducted with a TESCAN VEGA3 LMU microscope (EDS-Oxford), using AZTech (Advanced) software, SDD type detector of  $80 \text{ mm}^2$ , and tension of 10 kV.

Transmission electron microscopy (TEM) and selected area electron diffraction (SAED) studies were conducted with a JEOL JEM 1200 EX-II microscope with tension of 120 kV.

Diffuse reflectance ultraviolet-visible (DRUV-Vis) spectra were acquired at room temperature, between 200-800 nm using a Hewlett Packard 8452A diode array spectrophotometer and a Varian Cary 100 Bro UV-Vis spectrophotometer.

The artificial weathering test was performed in an ATLAS Ci400 Weather-Ometer camera, using a xenon lamp rated at 4500-6500 W (water cooled) with automatic irradiance of  $0.35 \pm 0.05 \text{ W m}^{-2}$  at 340 nm, black panel temperature of  $63 \pm 2 \text{ }^\circ\text{C}$ , cycle of 102 min of light and 18 min of light sprinkling, with internal and external borosilicate filter system.

To evaluate the effect of natural ester oil in the presence of  $Zn_2Al-N-AB$ , Rancimat tests were performed in a Metrohm 873 Biodiesel Rancimat instrument at  $130 \text{ }^\circ\text{C}$ , in air at flow rates of  $10 \text{ L h}^{-1}$ , according to the EN 14112 method.<sup>20</sup> In this method, an oil sample is heated in a thermostatic bath through which air is flowing. As the oil degrades, low molecular weight volatile acids are formed and transported to a vial containing distilled water and a conductivity electrode. The oxidation induction time (OIT) is the time between the start of the measurement and the onset of a rapid rise in conductivity.<sup>17</sup> The conductivity increases slowly during the early stages of the measurement but increases more rapidly after the OIT is reached. The OIT is easily identified in a plot of conductivity *versus* time by drawing tangents to the curve or by using the second derivative of the curve.<sup>17</sup> The effect of adding  $Zn_2Al-N-AB$  was evaluated by measuring the increase in the conductivity of the distilled water contained in the vial. The powder sample was mixed with  $3.00 \pm 0.01 \text{ g}$  of natural insulating oil (7 wt.%).

## Results and Discussion

### Layered double hydroxides

The XRD patterns of  $Zn_2Al-Cl$  and  $Zn_2Al-NO_3$  precursors and the LDH after the exchange reactions

(Zn<sub>2</sub>Al-Cl-AB and Zn<sub>2</sub>Al-N-AB) (Figure 2) presented typical profiles of LDH with intense and sharp reflection at low  $2\theta$  values and less intense reflections at higher angular values. The precursors Zn<sub>2</sub>Al-NO<sub>3</sub> and Zn<sub>2</sub>Al-Cl exhibited strong reflections indexed according to hexagonal cells as (003), (006) and (009),<sup>11</sup> with calculated basal spacings of 7.74 and 9.10 Å, respectively. A small unknown impurity could also be seen at  $2\theta = 29.5^\circ$  (Figure 2a). In the XRD pattern of Zn<sub>2</sub>Al-N-AB (Figure 2b), an increase of the basal distance was observed due to the *p*-AB intercalation. The basal distance increased to 15.2 Å, which is greater than the simple sum of the layers' thicknesses (around 4.8 Å)<sup>21,22</sup> with the length of the *p*-AB anion (calculated as 6.8 Å). The XRD of Zn<sub>2</sub>Al-Cl-AB (Figure 2d) indicated that the solid presented smaller particles after the modification through anion exchange, since in Zn<sub>2</sub>Al-Cl-AB XRD, the reflections were wider than those of the unmodified LDHs. As Zn<sub>2</sub>Al-Cl-AB has almost double the basal parameter of Zn<sub>2</sub>Al-Cl, the material also was detected as a mixture of Zn<sub>2</sub>Al-Cl-AB with non-exchanged Zn<sub>2</sub>Al-Cl domains by the intensity of the second order peak. Besides this, the solid Zn<sub>2</sub>Al-N-AB showed higher crystallinity, so we decided to continue working with this compound. The basal distance observed for both intercalated samples may mean that the *p*-AB anions are arranged in between the inorganic layers so that they displace the carboxylate functional groups upward and downward, but still arrange the aromatic rings mutually by  $\pi$ - $\pi$  interactions, and their amino groups through H-bonds.

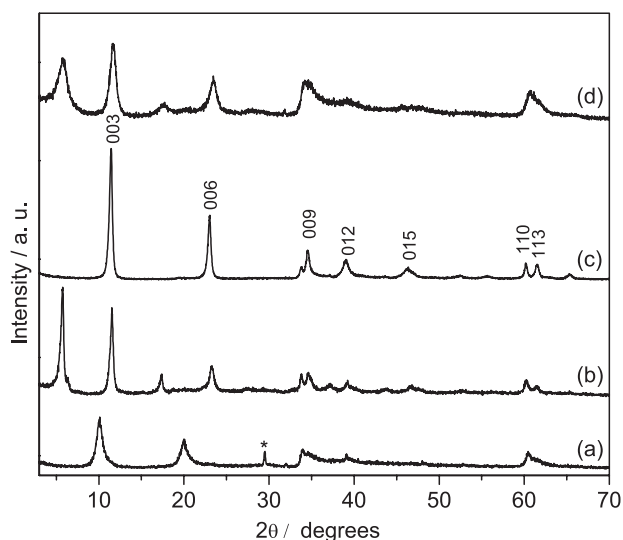


**Figure 2.** XRD patterns of Zn<sub>2</sub>Al-NO<sub>3</sub> (a), Zn<sub>2</sub>Al-N-AB (b), Zn<sub>2</sub>Al-Cl (c) and Zn<sub>2</sub>Al-Cl-AB (d). \*Unknown impurity.

Many papers<sup>10,14,16,23-25</sup> have been published regarding the structure of LDHs intercalated with *p*-AB anions, and the discussion is of great interest. In general, LDHs interact

with the intercalated ions through electrostatic van der Waals forces (a negatively charged ion with a positively charged layer), involving no formation of chemical bonds, but only the physisorption of the guest species onto the layer.<sup>23</sup> Although grafting reactions (formation of chemical bonds between the ions and the layer) are common in layered hydroxide salts (LHSs), this reaction usually needs an excess of energy (heating) to occur, especially in LDHs.<sup>16,21,23</sup> Many works investigating zinc LHSs interacting with the *p*-AB intercalated anions (and similar species) have been published.<sup>24-27</sup>

However, here we paid particular attention to the results of Conterosito *et al.*<sup>28</sup> who reported that when *p*-AB anions are intercalated in zinc LDHs, they coordinate to the metal site through a covalent bond with no need of heating the system, as would be expected. This model suggests that the *p*-AB anions are not in an interdigitated arrangement as other researchers have claimed, but in such a way that the ions of the lower layer interact with other ions of the lower layer through  $\pi$ - $\pi$  forces, and with the ions of the upper layer with H-bonds in a N-H...N network. As the intercalated ions are coordinated to the trivalent aluminum site by only one oxygen atom of the carboxylate group, this makes the anion as a whole bend at an angle with respect to the normal to the layer, so the interlayer distance may be smaller than the length of a *p*-AB bilayer, as seen in the XRD results. The monografted *p*-AB anions can also be observed through the FTIR results (Figure S1, Supplementary Information (SI) section), when studying the difference of symmetric and antisymmetric  $\nu(\text{C}=\text{O})$  modes.<sup>29</sup> This discussion is of great interest when studying this kind of materials, since they do not usually show the formation of covalent bonds between the inorganic layers and the intercalated anion. The spatial configuration of the intercalated anionic species leads to other phenomena seen in these materials, such as the basal spacing and the cell parameters.

Taking into consideration the basal spacing of 15.2 Å and the length of an inorganic layer as 4.8 Å, one can conclude that the *p*-AB anions in the bilayers are at an angle between 40.9 and 60° with respect to the normal to the layer, as a result of phenomena such as anion single grafting reactions, steric effects between the layer and the tilted anions, and the intermolecular interactions between the intercalated ions ( $\pi$ - $\pi$  and H-interactions). The occurrence of double grafting may be also possible in LHSs, leading to an ion bonded to the layer by both oxygen atoms of the carboxylate group. That would, however, not be possible in LDHs considering the need of M<sup>3+</sup> sites for the reaction to take place, sites that are usually far from each other in an ordered system with 2:1 ratio (Zn:Al), as is the case of Zn<sub>2</sub>Al LDH.

The augment in the  $d$  parameter seen in the XRD pattern nonetheless indicates the successful  $p$ -AB exchange of the nitrate in  $\text{Zn}_2\text{Al-N-AB}$ , while in the case of  $\text{Zn}_2\text{Al-Cl-AB}$ , the exchange reaction was only partial.

TGA measurements of anhydrous PABA (Figure 3A, curve a) presented two main stages of mass loss, both attributed to the oxidation of the organic material. The main event was in the region of 200 °C, with a mass loss of 93.8% at 300 °C, and the second at around 550 °C, with an accumulated mass loss of 99.8%, indicating the absence of any inorganic components (deviation of 0.2%).

The decomposition of  $\text{Zn}_2\text{Al-NO}_3$  (Figure 3A, curve c) occurred with three thermal events: 11.9% mass loss between room temperature and 187 °C, 13.3% mass loss between 187 and 273 °C, and 21.01% at 1000 °C. The residue ( $\text{ZnAl}_2\text{O}_4 + \text{ZnO}$ ) of 54.39% at 1000 °C (61.7% in anhydrous form) was relatively far from the ideal anhydrous formula from  $\text{Zn}_{0.67}\text{Al}_{0.33}(\text{OH})_2(\text{NO}_3)_{0.33}$  (66.57%). The deviation of around 7.9% is attributed to the difficulty of finding a temperature where the anhydrous material is obtained and the presence of impurities, as attested by the XRD curves, on the other hand, for simple anions like nitrate the mass difference may be caused due to that not all anion exchange position are occupied by nitrate anions (Figure 2a).

$\text{Zn}_2\text{Al-Cl}$ 's decomposition profile (Figure 3A, curve d) shows three thermal events: loss of physisorbed and intercalated water molecules (8.87% mass loss at 171 °C), dehydroxylation around 171-384 °C with 15.53% loss, and formation of residue with 36.76% total mass loss at 1000 °C. Considering the anhydrous phase at 171 °C with a residual mass in anhydrous form of 72.5%, this is close to the expected 69.8% according to the ideal formula  $\text{Zn}_{0.67}\text{Al}_{0.33}(\text{OH})_2\text{Cl}_{0.33}$ , with a deviation of 4.5%.

Thermal analysis data of  $\text{ZnAl-N-AB}$  (Figures 3A, curve b, and 3B) indicated the occurrence of a mass loss of 7.7% up to 120 °C, due to release of physisorbed and intercalated water. Between 120 and 292 °C the dehydroxylation of the layered material was observed, indicated by mass loss of 13.07%. Then a mass loss of 29.82% was observed up to 1000 °C, attributed to the oxidation of the organic matter. The composition of the LDH, according to this analysis, was  $\text{Zn}_{0.67}\text{Al}_{0.33}(\text{OH})_2(p\text{-AB})_{0.33}$ , where the predicted residue of 54.64% in dry basis matches the obtained value (54.20%) with a deviation of 0.8%. The content of water was also determined at 120 °C, given the hydrated formula of  $\text{Zn}_{0.67}\text{Al}_{0.33}(\text{OH})_2(p\text{-AB})_{0.33} \cdot 0.61\text{H}_2\text{O}$ .

An important parameter in the TGA analysis of  $\text{Zn}_2\text{Al-N-AB}$  showed that its thermal stability was improved compared to the PABA alone. According to Wang *et al.*,<sup>2</sup> for industrial purposes, polymer processing uses temperatures close to 180 °C, so it would not be recommended to use the PABA as additive directly in the polymer matrix.

The TEM images of the LDHs (Figure 4) indicated nanometric platelet-like particles, typical of LDH structures. The SAED spectra of single crystals showed a hexagonal structure projection, in accordance with the literature.<sup>14</sup>

The SAED pattern indicates that after anion exchange of  $\text{Zn}_2\text{Al-Cl}$  and  $\text{Zn}_2\text{Al-NO}_3$  with the  $p$ -AB anions, the structure has a crystal order similar to the starting layered material ( $a = b$  ca. 3.06 Å). The cell parameter found is close to the  $d_{(110)}$  peak value found through XRD ( $2d_{(110)} = 3.07$  Å), disregarding the superstructure (Figure 2). As observed in TEM images and SAED spectra (Figures 4c and 4d), the  $\text{Zn}_2\text{Al-N-AB}$  structure showed an amorphous region and a pattern of rings, due to the decomposition caused by the electron beam. The information about the parameters

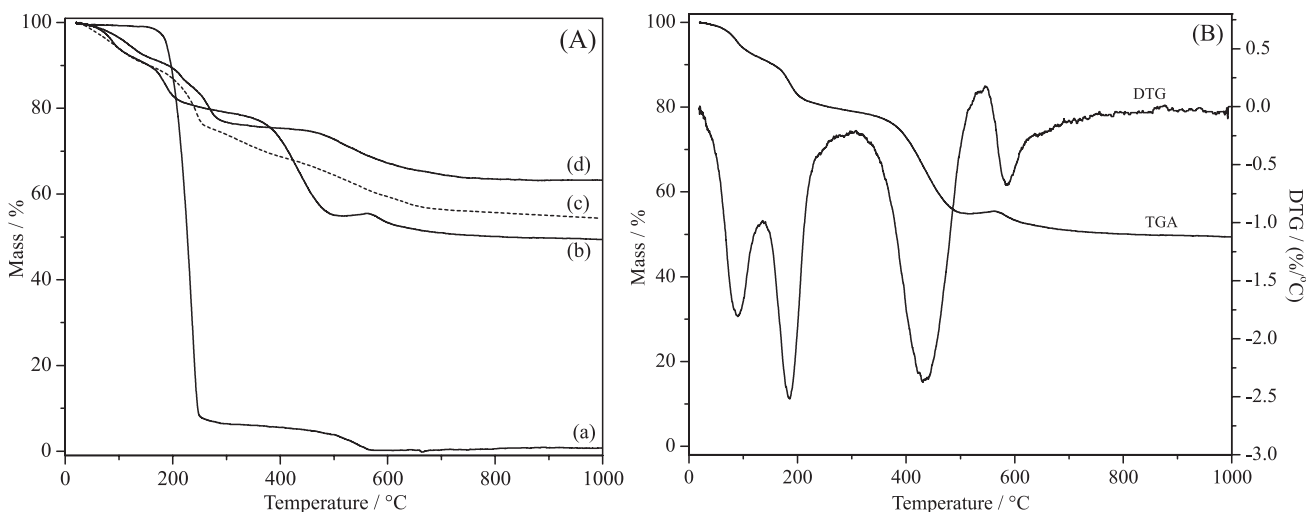


**Figure 3.** (A) TGA curves of (a) PABA; (b)  $\text{Zn}_2\text{Al-N-AB}$ ; (c)  $\text{Zn}_2\text{Al-NO}_3$ ; and (d)  $\text{Zn}_2\text{Al-Cl}$ ; (B) TGA/DTG curves of  $\text{Zn}_2\text{Al-N-AB}$ .

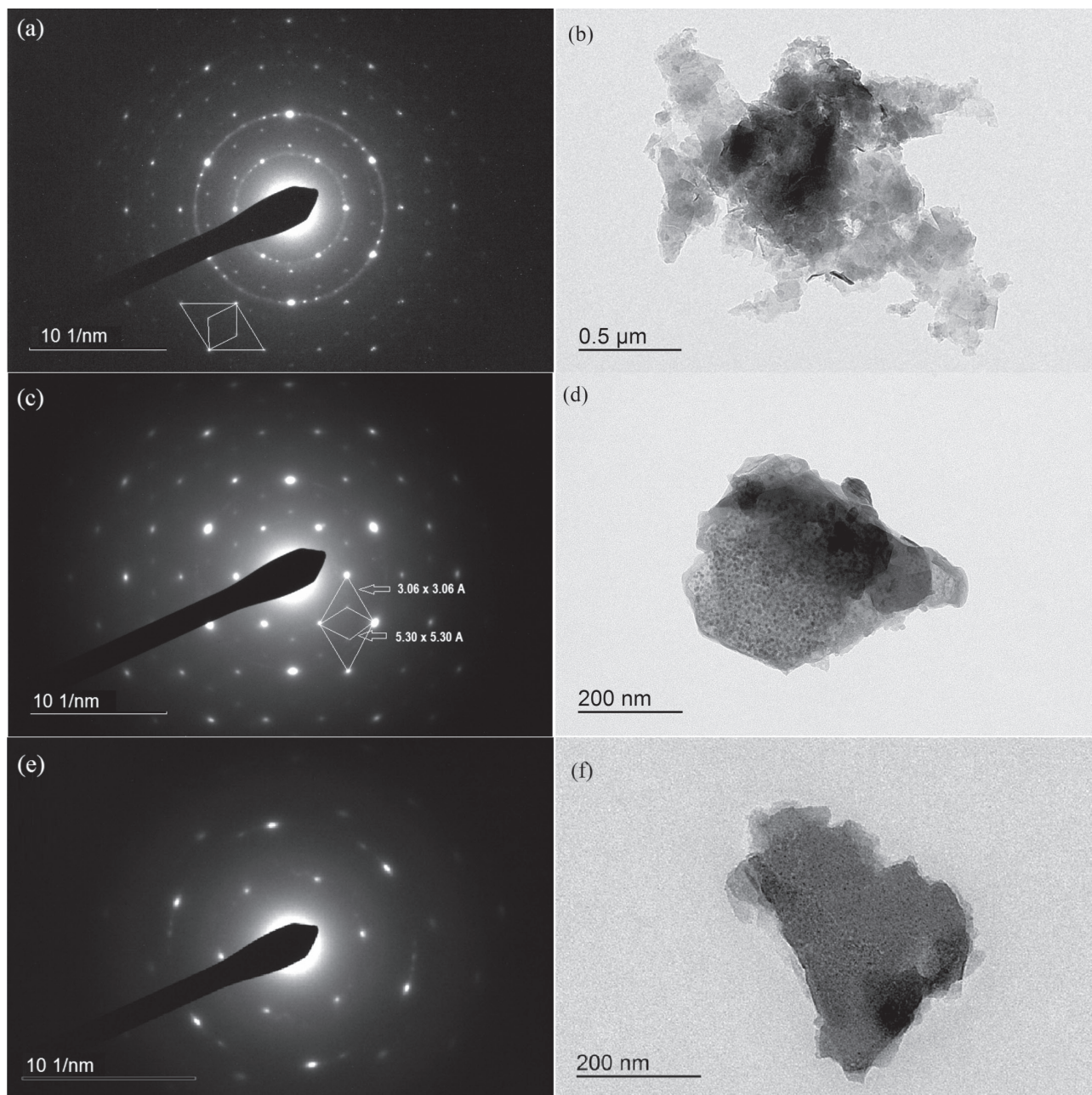


**Figure 4.** SAED spectra of (a) Zn<sub>2</sub>Al-NO<sub>3</sub>; (c) Zn<sub>2</sub>Al-N-AB and (e) Zn<sub>2</sub>Al-Cl; and the corresponding TEM images (b, d and f, respectively).

*a* and *b* indicated the existence of a superstructure with  $a \times \sqrt{3} = 5.30 \text{ \AA}$  in Zn<sub>2</sub>Al-N-AB (Figure 4c), indicating the order of the Al<sup>3+</sup> atoms in the layers, typical of LDH with M<sup>2+</sup>:M<sup>3+</sup> molar ratios of 2:1. The same superstructure was also observed for Zn<sub>2</sub>Al-NO<sub>3</sub> (Figure 4a).

Considering that the *p*-AB anions neutralize the excess positive charge generated by the Al<sup>3+</sup> metal cations, the distances between the intercalated ions should be similar. With respect to this distance,  $\pi$ - $\pi$  interactions have a strong stabilizing character of aromatic rings in T-shaped configurations, and a little less in the sandwich configuration.<sup>24</sup> Figure S2 (SI section) shows more about

the morphology of the synthesized LDHs in SEM images and EDS spectra, confirming the ion exchange.

The DRUV-Vis spectra of the Zn<sub>2</sub>Al LDHs as well as sodium *p*-aminobenzoate are shown in Figure 5.

PABA is an aromatic organic molecule with carboxylate and amino functional groups, so it presents UV absorption between 215 and 337 nm due to  $n$ - $\pi^*$  and  $\pi$ - $\pi^*$  transitions. Sodium *p*-aminobenzoate showed peaks with maxima at 229 and 294 nm. Zn<sub>2</sub>Al-Cl LDH showed maximum UV absorptions at 233, 350 and 417 nm with a broadening in the UVA and visible region, while Zn<sub>2</sub>Al-NO<sub>3</sub> showed maxima at 227 and 303 nm and transparency in the visible

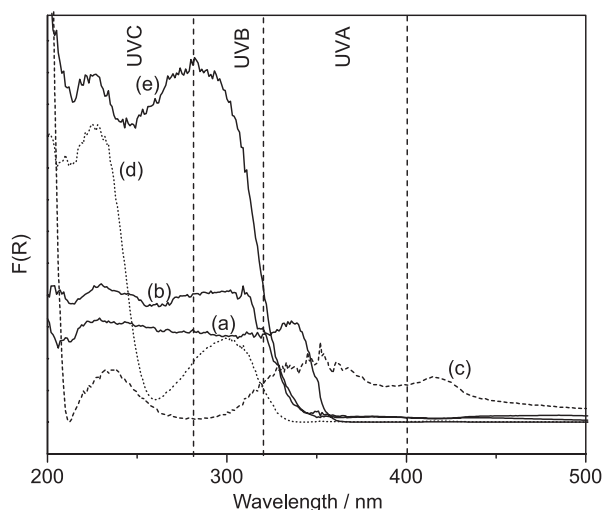


**Figure 5.** DRUV-Vis of (a) *p*-aminobenzoic acid; (b) sodium *p*-aminobenzoate; (c)  $\text{Zn}_2\text{Al-Cl}$ ; (d)  $\text{Zn}_2\text{Al-NO}_3$  and (e)  $\text{Zn}_2\text{Al-N-AB}$  LDH, plotted as the Kubelka-Munk function of reflectance,  $R$ .

region. After intercalation,  $\text{Zn}_2\text{Al-N-AB}$  LDH presented maximum absorption in the most energetic UVC and UVB regions at 224 and 286 nm, respectively, and with a broadening in the UVA and visible regions. LDHs showed improved UV absorption property compared with the PABA alone.

#### Polymer nanocomposites

Analyzing the SEM images of the cryogenic fracture of the samples LDPE/LDH  $\text{Zn}_2\text{Al-AB}$  4 wt.% (50,000 $\times$ ) (Figure S3a, SI section) and LDPE/LDH  $\text{Zn}_2\text{Al-N}$  4 wt.% (50,000 $\times$ ) (Figure S3b, SI section), relatively homogeneous materials were observed and the LDH particles are clearly imbedded in the polymeric matrix. A close inspection indicated that in both cases after the cryogenic fracture, some particles are detached leaving holes, as expected for the good adhesion between the LDH particles and the polymeric matrix. After these results, the neat LDPE and LDPE/ $\text{Zn}_2\text{Al}$  LDH nanocomposite samples were prepared through the injection molding method. In the case of semi-

crystalline polymers, such as polyethylene, it is important to know the temperatures of melting ( $T_m$ ) and crystallization ( $T_c$ ), since these parameters are associated with routine industrial processes where these kinds of compounds are of great interest. Table 1 shows the parameters for nanocomposites obtained from DSC analysis (Figure S4, SI section) during the first cooling and the second heating processes.

As observed, the nanocomposites LDPE/ $\text{Zn}_2\text{Al-NO}_3$  5 wt.% and LDPE/ $\text{Zn}_2\text{Al-N-AB}$  5 wt.% showed a slight increase of  $T_c$  compared to neat LDPE. This result shows that the polymer interacts strongly with the filler, probably due to the addition of the compatibilizing agent, which may facilitate crystallization in the cooling process. The  $T_m$  parameter increased slightly when the AB intercalated LDH was used as filler in LDPE. It is necessary to consider addition of the plastic modifier, which promotes better interaction between the polar (LDH) and nonpolar (LDPE) components in the nanocomposite, due to the polar character of the anhydride group in the maleic anhydride and the strong van der Waals interactions between the polymer, the polymer modifier and the composite matrix.

It can be observed (Figure S5, SI section) that the enthalpy of crystallization and melting ( $\Delta H_c$ ,  $\Delta H_m$ ) decreased to some extent when the LDHs were used as fillers in the matrix, even when dilution effects of the polymer with the filler are taken into consideration (correcting the values as if they were due to 100% polymer). These parameters are related to the crystallinity of the nanocomposite and suggest that the slightly changed degree of crystallinity was lower for  $\text{Zn}_2\text{Al-N-AB}$  than  $\text{Zn}_2\text{Al-NO}_3$  LDHs, when compared to neat LDPE. The degree of crystallization ( $X_c$ ) of neat LDPE and LDPE/LDH nanocomposites were calculated with equation 1, in which the enthalpy of crystallization of pure polyethylene ( $\Delta H_c^0$ ) is 293 J g $^{-1}$ .<sup>30</sup> The lower crystallization temperature of the polymer was expected since the addition of the load and the compatibilizing agent should promote obstacles to the crystallization of the bulk polymer, leading to the creation of smaller polymer crystal domains in

**Table 1.** Melting ( $T_m$ ) and crystallization ( $T_c$ ) temperatures and the corresponding enthalpies ( $\Delta H_m$  and  $\Delta H_c$ ) of neat LDPE and LDPE nanocomposites, obtained by DSC analysis. In brackets, the corrected values due to dilution of the polymer considering 100% LDPE in the nanocomposites

Compound	$T_c$ / $^{\circ}\text{C}$	$T_m$ / $^{\circ}\text{C}$	$\Delta H_c$ / (J g $^{-1}$ )	$\Delta H_m$ / (J g $^{-1}$ )	$X_c$
LDPE	106.8	119.4	-137.0	136.3	46.8
LDPE/PABA	107.2	118.8	-126.9 (-133.6)	128.4 (135.2)	43.3 (45.6)
LDPE/ $\text{Zn}_2\text{Al-N}$ 5 wt.%	108.3	119.7	-121.0 (-128.4)	123.2 (129.7)	41.2 (43.4)
LDPE/ $\text{Zn}_2\text{Al-N-AB}$ 5 wt.%	109.0	120.2	-122.9 (-129.4)	125.0 (131.6)	41.9 (44.1)

$T_c$ : crystallization temperature;  $T_m$ : melting temperature;  $\Delta H_c$ : crystallization enthalpy;  $\Delta H_m$ : melting enthalpy;  $X_c$ : degree of crystallization; LDPE: low-density polyethylene; PABA: *p*-aminobenzoic acid.

the structure compared to the pure LDPE, which would crystallize as a whole.

$$X_c(\%) = \frac{\Delta H_c}{\Delta H_c^0} \times 100 \quad (1)$$

UV absorption of LDPE nanocomposites and neat LDPE were compared (Figure 6).

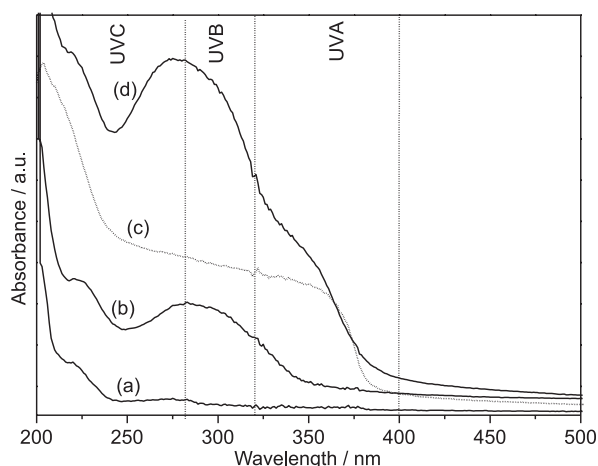


**Figure 6.** UV-Vis spectra of (a) neat LDPE; (b) LDPE/Zn<sub>2</sub>Al-NO<sub>3</sub> 5 wt.%; (c) LDPE/PABA 5 wt.%; (d) LDPE/Zn<sub>2</sub>Al-N-AB 5 wt.%.

The UV spectra of neat LDPE showed low UV absorption capacity in the UVC region, with a maximum at 219 nm. The nanocomposite with PABA as filler in LDPE had higher UV absorption than LDPE between 200–400 nm, due to the effect of the organic absorber molecule. When the LDH was used as filler, the nanocomposite showed enhanced UV absorption capacity, with maximum at 276 nm, covering the region between 200 and 400 nm. This UV absorption of the nanocomposite was stronger than its precursors, increasing from 6% for neat LDPE to 89% for LDPE/Zn<sub>2</sub>Al-N-AB 5 wt.% at 276 nm.

UV-Vis absorption thus demonstrated that LDPE/Zn<sub>2</sub>Al nanocomposites have better absorbing capacity. However, to see if this absorption really enhances the anti-photoaging performance of LDPE, it was necessary to evaluate the effect of weathering on polyethylene degradation.

#### Accelerated aging test (weathering)

The nanocomposites FTIR spectra (Figure 7) indicated bands around 3400 cm<sup>-1</sup>, attributed to ν(O–H).

Vibration of the ν(–CH<sub>2</sub>–) bond band of LDPE were observed at 1470 cm<sup>-1</sup>. After weathering, a band at 1715 cm<sup>-1</sup>, attributed to ν(C=O) of ketone functional groups from oxidation products appeared.<sup>29,30</sup> The characteristic bands from the PABA compound at 1603 and 1528 cm<sup>-1</sup> were attributed to ν(C=O) and ν(C=C) of the aromatic ring<sup>14</sup>

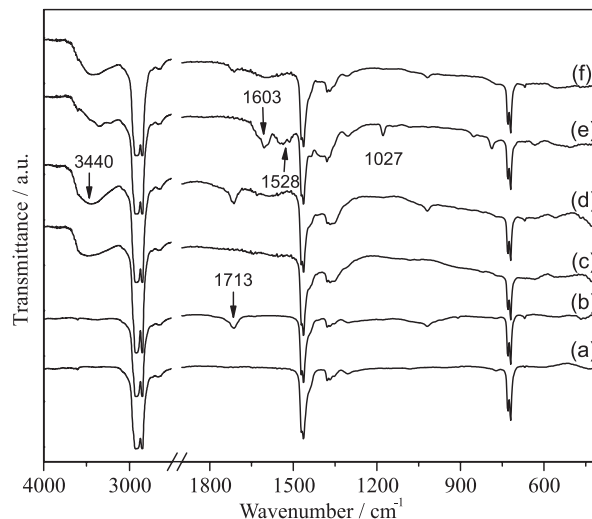


**Figure 7.** FTIR spectra of (a) LDPE; (b) LDPE after weathering; (c) LDPE/Zn<sub>2</sub>Al-NO<sub>3</sub> 5 wt.%; (d) LDPE/Zn<sub>2</sub>Al-NO<sub>3</sub> 5 wt.% after weathering; (e) LDPE/Zn<sub>2</sub>Al-N-AB 5 wt.%; and (f) LDPE/Zn<sub>2</sub>Al-N-AB 5 wt.% after weathering.

and decreased in intensity after weathering for 300 h. The FTIR results showed that the Zn<sub>2</sub>Al-N-AB structure was still present in the polymer but was partially delaminated, as indicated by the XRD pattern (Figure S5, SI section).

To observe the effect of the weathering on nanocomposites, a band analysis between aged films with filler loading of 5 wt.% was carried out. As references, the stretching band from ν(–CH<sub>2</sub>–) bonds (which do not undergo deformation by weathering), and the band from ν(C=O) (attributed to oxidation compounds generated due to polymer degradation) were chosen.<sup>3,4,31</sup> The obtained band ratios showed reductions of oxidation products of 25 and 76% when Zn<sub>2</sub>Al-NO<sub>3</sub> and Zn<sub>2</sub>Al-N-AB LDH were used as fillers in LDPE to produce the nanocomposite. This can mean that Zn<sub>2</sub>Al LDH has a protective effect against polyethylene oxidation, where the presence of the organic anion more efficiently inhibits the formation of carbonyl groups during weathering. Both LDHs have potential application in the field of LDPE as efficient UV-shielding material (Table 2).

The weathering did not change the basal spacing in the mixed LDH (Figure S5, SI section), (d ca. 15.2 Å). The

**Table 2.** Band area ratios (1715 cm<sup>-1</sup>:1463 cm<sup>-1</sup>) for Zn<sub>2</sub>Al-NO<sub>3</sub> and Zn<sub>2</sub>Al-N-AB LDH

Sample	ν(C=O):ν(–CH <sub>2</sub> –) area ratio / a.u.
LDPE	0.045
LDPE 300 h	0.360
LDPE/Zn <sub>2</sub> Al-NO <sub>3</sub> 5 wt.% 300 h	0.270
LDPE/Zn <sub>2</sub> Al-N-AB 5 wt.% 300 h	0.088

LDPE: low-density polyethylene.

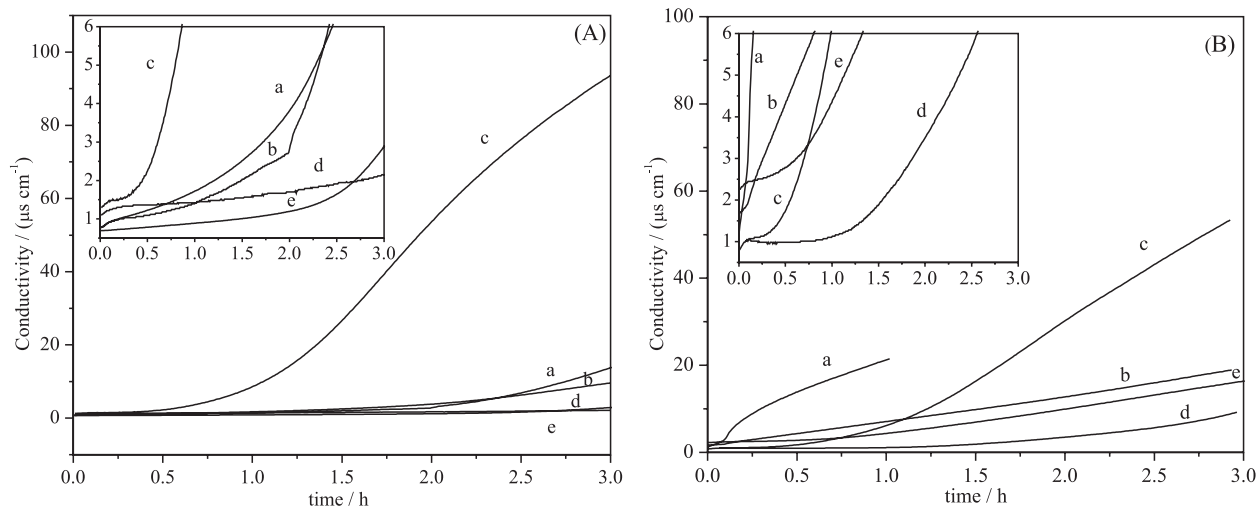


**Figure 8.** Measured conductivity versus time plots for (A) FR3 and (B) castor oil, (a) without additive and in presence of (b) PABA; (c)  $\text{Zn}_2\text{Al-NO}_3$ ; (d)  $\text{Zn}_2\text{Al-Cl}$  and (e)  $\text{Zn}_2\text{Al-N-AB}$ .

XRD results also showed that the LDH in the polymer after extrusion was exfoliated throughout the material, as can be seen by the absence of the characteristic (00 $l$ ) peaks at low angles. The same phenomenon is not seen in the  $\text{ZnAl-NO}_3$ , perhaps due to the inorganic nature of the intercalated species and their affinity to the polymer, which is expected to be greater with *p*-AB than with nitrate.

#### Natural insulating oils

Natural vegetable insulating oils are commonly used in distribution and power transformer applications as alternatives to mineral oil, due to their better environmental properties.<sup>32</sup> Two natural insulating oils, FR3 and castor oil, in the presence of  $\text{Zn}_2\text{Al-NO}_3$  and  $\text{Zn}_2\text{Al-N-AB}$ , were analyzed through Rancimat equipment at 130 °C and airflow of 10 L h<sup>-1</sup> (Figure 8).

Results showed that conductivity ( $\mu\text{S cm}^{-1}$ ) changed when LDH/UV absorber was used as additive in the oil. Under operational conditions, the insulating oils can degrade due to oxidation, which can cause loss of insulating properties.<sup>32,33</sup> In the accelerated aging test, volatile products are generated as a secondary reaction due to the oxidation process of fatty acids. The presence of these compounds increases the conductivity measured in aqueous solutions. Detected OIT until secondary reaction products (polar products of oxidation) is a measure of the time that passes until the oxidation takes place, a property that has a direct relation with conductivity.<sup>17,33</sup> According to the results, the OIT was higher in presence of  $\text{Zn}_2\text{Al-N-AB}$  (Figure 8) and the conductivity decreased compared to the pure oil. As observed, when an organic UV absorber was intercalated in  $\text{Zn}_2\text{Al}$  and mixed with the vegetable insulating oil, the oxidation was lower compared to both oils without additives,

indicating  $\text{Zn}_2\text{Al-N-AB}$  as a possible additive to decrease the oxidation due to air presence, and therefore improving the oxidation stability of the evaluated natural insulating oils.

#### Conclusions

The co-precipitation method was used to synthesize LDHs of  $\text{Zn}_2\text{Al}$  intercalated with chloride and nitrate. While the exchange of chloride with *p*-AB was partial, nitrate was fully exchanged with *p*-AB at 60 °C after 5 days of reaction.

The intercalation of the *p*-AB anions was first verified using an X-ray diffraction, due to the basal spacing increases of  $\text{Zn}_2\text{Al-Cl}$  and  $\text{Zn}_2\text{Al-NO}_3$  from 7.74 and 9.2 to 15.2 Å, respectively. FTIR, TGA and SEM/EDS characterization techniques were used to confirm the presence of *p*-AB anions in LDH.

The synthesized  $\text{Zn}_2\text{Al-N-AB}$  showed a hexagonal structure projection in the SAED with cell parameter values  $a = b = 3.06$  Å, with a superstructure of  $a \times \sqrt{3} = 5.30$  Å, due to the ordering of the  $\text{M}^{3+}$  metals in the layers. These values are close to the cell parameter value found with the  $d_{(110)}$  reflection through XRD ( $2a = 3.07$  Å).

$\text{Zn}_2\text{Al-N-AB}$ ,  $\text{Zn}_2\text{Al-Cl}$  and  $\text{Zn}_2\text{Al-NO}_3$  were able to absorb radiation in regions of higher energy (UVC and UVB).  $\text{Zn}_2\text{Al-NO}_3$  and  $\text{Zn}_2\text{Al-N-AB}$  were used as fillers in low-density polyethylene (LDPE), producing homogeneous polymer nanocomposite materials by injection molding. The presence of LDH was verified through FTIR, XRD, SEM and TGA characterization.

TGA of the nanocomposite LDPE/ $\text{Zn}_2\text{Al-N-AB}$  showed that thermal stability was close to that of neat LDPE, using the filler at 1 wt.%. The temperatures to lose 10 and 50% of material changed from 452 and 476 °C for LDPE to 446 and 472 °C for LDPE/ $\text{Zn}_2\text{Al-N-AB}$ . The melting and

crystallization temperatures of the nanocomposites were slightly increased in LDPE/Zn<sub>2</sub>Al. To compare the neat LDPE with LDPE nanocomposites, dilution of the quantity of polymer in the nanocomposite can be considered to correct the thermal parameters.

The nanocomposites showed a higher UV absorption region than neat LDPE, covering the region between 400-200 nm and broadening to the visible region. After a weathering test, nanocomposites generated a lower ratio of carbonyl groups than the neat LDPE under the same conditions. Zn<sub>2</sub>Al-N-AB showed better protective ability for LDPE; hence it is possible to conclude that Zn<sub>2</sub>Al LDHs have potential applications as UV absorbers in polymers. Zn<sub>2</sub>Al-N-AB showed these properties due to the interactions the intercalated PABA anions had with light.

Preliminary Rancimat testing also showed that Zn<sub>2</sub>Al-N-AB LDH could be used as additive for natural insulating esters, since the oxidation stability of the oil was improved when the UV absorber was intercalated between the LDH layers.

## Supplementary Information

Supplementary information (XRD patterns, FTIR spectra, SEM images, EDS analysis, TGA/DSC analysis of the LDHs and LDPE composites) is available free of charge at <http://jbcs.sbq.org.br> as PDF file.

## Acknowledgments

The authors thank CAPES (Coordenação de Aperfeiçoamento de Pessoal de Nível Superior, Finance code 001), CNPq (Conselho Nacional de Desenvolvimento Científico e Tecnológico, projects Nos. 303846/2014-3 and 40117-2016-9), and FINEP (Financiadora de Estudos e Projetos) for financial support, and Centro de Microscopia Eletrônica (CEM/UFPR) for the SEM and SAED analyses. N. A. G. G. and G. M. S. thank CAPES for the PhD and master's scholarships.

## References

1. Albertsson, A. C.; Andersson, S. O.; Karlsson, S.; *Polym. Degrad. Stab.* **1987**, *18*, 73.
2. Wang, Q.; Wu, J.; Gao, Y.; Zhang, Z.; Wang, J.; Zhang, X.; Yan, X.; Umar, A.; Guo, Z.; O'Hare, D.; *RSC Adv.* **2013**, *3*, 26017.
3. Yousif, E.; Haddad, R.; *SpringerPlus* **2013**, *2*, DOI 10.1186/2193-1801-2-398.
4. Ojha, N.; Pradhan, N.; Singh, S.; Barla, A.; Shrivastava, A.; Khatua, P.; Rai, V.; Bose, S.; *Sci. Rep.* **2017**, *7*, DOI 10.1038/srep39515.
5. Sheela, T.; Bhajantri, R. F.; Ravindrachary, V.; Rathod, S. G.; Pujari, P. K.; Poojary, B.; Somashekar, R.; *Radiat. Phys. Chem.* **2014**, *103*, 4.
6. Kamweru, K. P.; Ndiritu, G. F.; Kinyanjui, T.; Muthui, W. Z.; Ngumbu, G. R.; Odhiambo, M. P.; *Int. J. Phys. Sci.* **2014**, *9*, 545.
7. Basu, D.; Das, A.; Stöckelhuber, K. W.; Wagenknecht, U.; Heinrich, G.; *J. Appl. Polym. Sci.* **2014**, *39*, 594.
8. Wang, Q.; O'Hare, D.; *Chem. Rev.* **2012**, *112*, 4124.
9. Sotiles, A. R.; Baika, L. M.; Grassi, M. T.; Wypych, F.; *J. Am. Chem. Soc.* **2019**, *141*, 531.
10. Li, Y.; Li, S.; Zhang, Y.; Yu, M.; Liu, J.; *J. Alloys Compd.* **2015**, *630*, 29.
11. Wang, X.; Spörer, Y.; Leuteritz, A.; Kuehnert, I.; Wagenknecht, U.; Heinrich, G.; Wang, D. Y.; *RSC Adv.* **2015**, *5*, 78979.
12. Camargo, P. H. C.; Satyanarayana, K. G.; Wypych, F.; *Mater. Res.* **2009**, *12*, 1.
13. Purohit, P. J.; Wang, D. Y.; Emmerling, F.; Thünemann, A. F.; Heinrich, G.; Schönhals, A.; *Polymer* **2012**, *53*, 2245.
14. Roto, K.; Iqmal, T.; Mustofa, M.; *Indones. J. Chem.* **2007**, *7*, 1.
15. Zimmermann, A.; Jaeger, S.; Zawadzki, S. F.; Wypych, F.; *J. Polym. Res.* **2013**, *20*, DOI 10.1007/s10965-013-0224-3.
16. Gomez, N. A. G.; Maruyama, S. A.; Leuteritz, A.; Wypych, F.; *Polym. Bull.* **2019**, DOI 10.1007/s00289-019-02742-x.
17. Wilhelm, H. M.; Fernandes, P. O.; Feitosa, L. G.; dos Santos, G. C.; Pont, G. D.; Balielo, A.; *IEEE Electr. Insul. Mag.* **2018**, *34*, 7.
18. Coelho, C.; Hennous, M.; Verney, V.; Leroux, F.; *RSC Adv.* **2012**, *2*, 5430.
19. Sisti, L.; Totaro, G.; Celli, A.; Diouf-Lewis, A.; Verney, V.; Leroux, F.; *J. Environ. Chem. Eng.* **2019**, *7*, 103026.
20. EN 14112: *Fat and Oil Derivatives. Fatty Acid Methyl Esters (FAME). Determination of Oxidation Stability (Accelerated Oxidation Test)*; European Committee for Standardization: Brussels, 2003.
21. Wypych, F.; Arizaga, G. G. C.; Gardolinski, J. E. F. C.; *J. Colloid Interface Sci.* **2005**, *283*, 130.
22. Carlino, S.; *Solid State Ionics* **1997**, *98*, 73.
23. Biswick, T.; Jones, W.; Pacula, A.; Serwicka, E.; Podobinski, J.; *Solid State Sci.* **2009**, *11*, 330.
24. Xing, L. L.; Yuan, B.; Hu, S. X.; Zhang, Y. D.; Lu, Y.; Mai, Z. H.; Li, M.; *J. Phys. Chem. C* **2008**, *112*, 3800.
25. Zhao, L.; Wang, H.; Wang, Y.; Miao, J.; Feng, Q.; *Chin. J. Chem.* **2011**, *29*, 1837.
26. Wypych, F.; Schreiner, W. H.; Marangoni, R.; *J. Colloid Interface Sci.* **2002**, *253*, 180.
27. Cursino, A. C. T.; Gardolinski, J. E. F. C.; Wypych, F.; *J. Colloid Interface Sci.* **2010**, *347*, 49.
28. Conterposito, E.; Croce, G.; Palin, L.; Pagano, C.; Perioli, L.; Viterbo, D.; Boccaleri, E.; Paul, G.; Milanesio, M.; *Phys. Chem. Chem. Phys.* **2013**, *15*, 13418.

29. Nakamoto, K.; *Infrared and Raman Spectra of Inorganic and Coordination Compounds*, 4<sup>th</sup> ed.; Wiley: New York, USA, 1986, ch. 2.
30. Morawiec, J.; Pawlak, A.; Slouf, M.; Galeski, A.; Piorowska, E.; Krasnikowa, N.; *Eur. Polym. J.* **2005**, *41*, 1115.
31. Gulmine, J. V.; Janissek, P. R.; Heise, H. M.; Akcelrud, L.; *Polym. Degrad. Stab.* **2003**, *79*, 385.
32. Gómez, N. A.; Wilhelm, H. M.; Santos, C. C.; Stocoo, G. B.; *IEEE Trans. Dielectr. Electr. Insul.* **2014**, *21*, 1071.
33. Araújo, S. V.; Rocha, B. S.; Murilo, F. T. L.; Rola, E. M.; Azevedo, C. S.; Cavalcante, C. L.; *Fuel Process. Technol.* **2011**, *92*, 1152.

Submitted: August 26, 2019

Published online: November 21, 2019

